

# A fast and robust approach to long-distance quantum communication with atomic ensembles

L. Jiang<sup>1</sup>, J. M. Taylor<sup>1,2,\*</sup>, M. D. Lukin<sup>1</sup>

<sup>1</sup>*Department of Physics, Harvard University, Cambridge, Massachusetts 02138*

<sup>2</sup>*Department of Physics, Massachusetts Institute of Technology, Cambridge, Massachusetts 02139*

Quantum communication holds promise for cryptography, teleportation of arbitrary quantum states, and violation of Bell's inequalities over long distances [1]. While commercial implementation of simple quantum communication protocols are well established [2, 3], attenuation in optical fibers makes longer distances exponentially challenging. Quantum repeaters [4, 5, 6] overcome the time overhead associated with fiber attenuation by using a quantum memory and local quantum operations. A simple implementation uses atomic ensembles and linear optics [7] (DLCZ). Motivated by experimental progress, here we develop an efficient scheme compatible with the active purification of arbitrary errors. Using similar resources as the DLCZ approach, our approach intrinsically purifies leakage out of the logical subspace and all errors within the logical subspace, leading to greatly improved performance in the presence of experimental inefficiencies. We find that about one, 1280 km-distant entangled pair per minute could be realized with a fidelity sufficient to violate Bell's inequality.

\* Correspondence should be addressed to J. M. T. (email: jmtaylor@mit.edu)

Several promising avenues for quantum repeater implementation include both atomic ensembles (DLCZ) and using few qubit quantum computers, such as neutral atoms in cavity QED [8, 9], ion traps [10] and solid-state single photon emitters [11]. Experimental progress [12, 13, 14] towards realization of DLCZ has been especially rapid, with many building blocks demonstrated in the laboratory. The experimental challenge is now shifting towards the realization of scalable quantum repeater systems which could yield a reasonable communication rate at continental distances ( $\gtrsim 1000\text{km}$ ). Thus, the DLCZ protocol should be examined and adapted to practical experimental considerations, allowing to remove imperfections such as the finite efficiency of retrieval and single-photon detection and fiber length fluctuations. Our approach re-envisioned DLCZ, keeping the experimental simplicity of the original scheme while avoiding fundamental difficulties due to these expected experimental imperfections.

The DLCZ scheme starts with entanglement generation (ENG) by counting the interfering Stokes photons scattered from a pair of distant atomic cells  $x$  and  $y$ . This generates an entangled state

$$|\xi_\phi\rangle_{x,y} = \left( \hat{S}_x^\dagger + e^{i\phi} \hat{S}_y^\dagger \right) / \sqrt{2} |\text{vac}\rangle_{x,y} , \quad (1)$$

with  $\hat{S}_x^\dagger$  and  $\hat{S}_y^\dagger$  for creation operators of spin-wave modes in two cells respectively, and  $\phi$  the phase difference between left and right channels for Stokes photons [15]. Then entanglement connection (ENC) [7] is performed on two pairs of entangled atomic cells  $|\xi_{\phi_1}\rangle_{x_L,y_C}$  and  $|\xi_{\phi_2}\rangle_{x_C,y_R}$ , obtaining a further separated entangled pair  $|\xi_{\phi_1+\phi_2}\rangle_{x_L,y_R}$  probabilistically. The ENC step provides built-in purification against many imperfections—photon loss, atomic excitation loss and dark counts all give null results. In the final step, post-selection is used to obtain

an effectively *polarization entangled state*

$$|\Psi^{PES}\rangle = e^{i\phi} \left( \hat{S}_{x_1}^\dagger \hat{S}_{y_2}^\dagger + \hat{S}_{x_2}^\dagger \hat{S}_{y_1}^\dagger \right) / \sqrt{2} |\text{vac}\rangle \quad (2)$$

from two parallel pairs  $|\xi_\phi\rangle_{x_1,y_1}$ ,  $|\xi_\phi\rangle_{x_2,y_2}$ , which overcomes static phase errors (time independent  $\phi$ 's).

For practical quantum communication, the bandwidth (entangled pairs per second) at long distances is the key metric for evaluating performance of the protocol. For DLCZ, imperfections can significantly reduce the bandwidth to unusably low rates. Non-ideal retrieval and detection efficiency,  $\eta < 1$ , leads to two kinds of errors: states with a large vacuum component and states with two or more excitations. The former slows down the scheme and the latter may induce errors within the logical subspace reducing the entanglement of the final pair. Upper bounds given in Ref. [7] were sufficient to prove that DLCZ scales sub-exponentially with respect to time, a huge improvement compared to the method of direct quantum communication in lossy channel. In terms of bandwidth, however, DLCZ does not produce sufficient numbers of entangled pairs for key generation within several weeks time given practical efficiencies (Fig. 2(b)).

We now consider a different approach in which two atomic cells are used at each node  $a$ , labeled  $(a, H)$  and  $(a, V)$ , to store one qubit,  $a$ . The qubit is defined as one single spin-wave excitation shared between two cells:

$$\{ |H\rangle_a = S_{a,H}^\dagger |\text{vac}\rangle, |V\rangle_a = S_{a,V}^\dagger |\text{vac}\rangle \} . \quad (3)$$

When the stored spin waves are converted back into photons, the photons have a polarization ( $H$  or  $V$ ) consistent with that stored in the originating cell. This qubit basis allows projective measurements along any qubit states, e.g.,  $|\pm\rangle \equiv (|H\rangle_a \pm |V\rangle_a) / \sqrt{2}$ , using linear optical operations and photon counting [17]. We will show that in this logical basis it is possible to perform entanglement purification (ENP) [6] to reduce errors within the logical

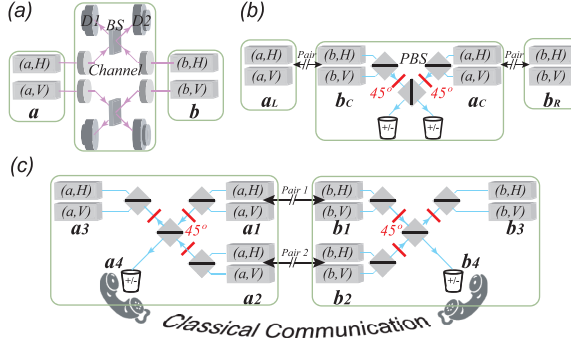


Figure 1: **Repeater components** (a) Entanglement generation (ENG). (b) Entanglement connection (ENC); indicated operations: retrieve  $b_C$  and  $a_C$  [additional  $45^\circ$  rotations only for the first level], join on polarizing beam splitter (PBS), detect in  $\pm$  basis conditioned on one photon per output, and finally adjust the phase. (c) Entanglement purification (ENP); indicated operations: retrieve  $a_1, b_1$  and  $a_2, b_2$  [additional  $45^\circ$  rotations to purify phase error], interfere  $a_1, a_2$  on PBS (same with  $b_1, b_2$ ), restore  $a_3, b_3$  conditioned on single photon at  $a_4$  and  $b_4$  respectively, and finally adjust the phase.

subspace, including phase fluctuation. Since ENP can suppress errors within the logical subspace which occur with probability  $q$  to  $O(q^2)$ , only a few ENP levels are needed to obtain high fidelity entanglement.

We now describe our procedures for ENG, ENC and ENP. ENG (Fig. 1(a)) is similar to that of DLCZ, but here *two* parallel entangled pairs are generated between  $a$  and  $b$ :

$$\begin{aligned} |\Psi^{ENG}\rangle_{a,b} &= |\xi_\phi\rangle_{(a,H)(b,H)}^+ |\xi_\phi\rangle_{(a,V)(b,V)}^+ \\ &= e^{i\phi} (|H\rangle_a |V\rangle_b + |V\rangle_a |H\rangle_b) + \\ &\quad |HV\rangle_a |\text{vac}\rangle_b + e^{2i\phi} |\text{vac}\rangle_a |HV\rangle_b . \end{aligned} \quad (4)$$

The entangled states are prepared in the quantum memory, so no simultaneity is required for creating the two states comprising  $|\Psi^{ENG}\rangle$ . For small excitation probability  $p_c$ , the whole generation only takes time  $O(1/p_c)$ , in contrast to  $O(1/p_c^2)$  for schemes requiring simultaneity, e.g., coupling between trapped atom and photon [10] or parametric down conversion [16]. Errors from multi-photon events occur only with probability  $p_c^2$ , and are considered in later analysis of imperfections.

The first level of ENC converts two  $|\Psi^{ENG}\rangle$  states (one between  $a_L$  and  $b_C$ , the other between  $a_C$  and  $b_R$ ) into polarization entangled states  $|\Phi^\pm\rangle_{ab} = |H\rangle_{a_L} |H\rangle_{b_R} + |V\rangle_{a_L} |V\rangle_{b_R}$ . Only four out of the sixteen terms in the Schmidt decomposition of  $|\Psi^{ENG}\rangle_{a_L b_C} |\Psi^{ENG}\rangle_{a_C b_R}$  have any contribution to the output state; the remainder are eliminated by projective measurement during ENC, reducing the probability of success for ENC from 1/2 to 1/8. At higher levels of ENC, the operations correspond to standard entanglement swapping [4, 5], where

$$|\Phi^\pm\rangle_{a_L b_C} \otimes |\Phi^\pm\rangle_{a_C b_R} \rightarrow |\Phi^\pm\rangle_{a_L b_R}$$

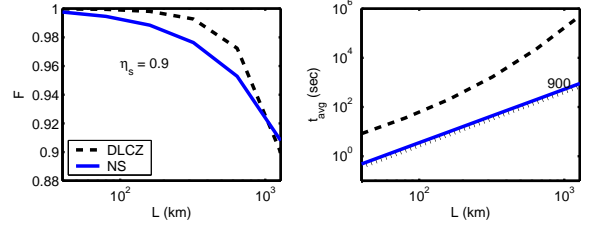


Figure 2: **Comparison between DLCZ scheme and new scheme (without ENP)** For each scheme, by choosing appropriate initial fidelity for elementary pairs, polarization entangled state with distance 1280km and fidelity  $F = 90\%$  (after post-selection) can be generated. (a) Fidelity profiles (solid: new scheme; dashed: DLCZ). (b) Average time profiles from simulations; dotted lines give the theoretical prediction from Eq.(A3). Both plots assume retrieval and detection efficiency  $\eta = 90\%$ .

leads to an entangled pair between  $L$  and  $R$  with probability 1/2, as detailed below. The ENC procedure is shown in Fig. 1(b) and detailed in Methods.

The third component is ENP (Fig. 1(c)) which obtains a high fidelity entangled pair from two pairs. Our procedure uses polarization entangled photons and is similar to what has already been experimentally investigated [16]. During entanglement purification of bit errors (bit-ENP), the qubits from two parallel pairs  $\rho_{a_1, b_1}$  and  $\rho_{a_2, b_2}$  are retrieved from the quantum memory and joined at PBSs. The photons for two upper outputs are stored into quantum memory  $a_3$  and  $b_3$ . The photons for the lower outputs  $a_4$  and  $b_4$  are counted in  $\{|+\rangle, |-\rangle\}$  basis. With probability 50%, there is exactly one photon at each lower output, and the purification is successful; otherwise two new pairs are created by restarting the process. If the two photons have orthogonal polarizations, a phase flip is applied to  $a_3$ . During purification of phase errors (phase-ENP), additional  $45^\circ$  rotations are applied to the retrieved qubits and the bit flip is replaced by the phase flip. The addition of  $45^\circ$  rotations effects the basis transform  $|\Phi^-\rangle \leftrightarrow |\Psi^+\rangle$ , leading to purification of errors of the other type. Bit and phase errors can be non-linearly suppressed to second order during bit-ENP and phase-ENP, respectively.[20]

The three components described above for quantum repeater protocol only use atomic cells, linear optics, and photon number resolving detectors. The duration of the retrieved anti-Stokes pulse can be made long ( $\gtrsim 1\mu\text{s}$ ) compared to detector recovery times by adjusting the intensity and duration of the retrieval pulse. This enables resolution of individual photons of the anti-Stokes pulse [19].

Based on the calculation of the success probability at each level of connection/purification, we can obtain the estimated average time for various schemes. In Fig. 2, we compare our approach to the DLCZ scheme. For the DLCZ scheme, the average generation time of distant pair scales *super-polynomially* (but still sub-exponentially)

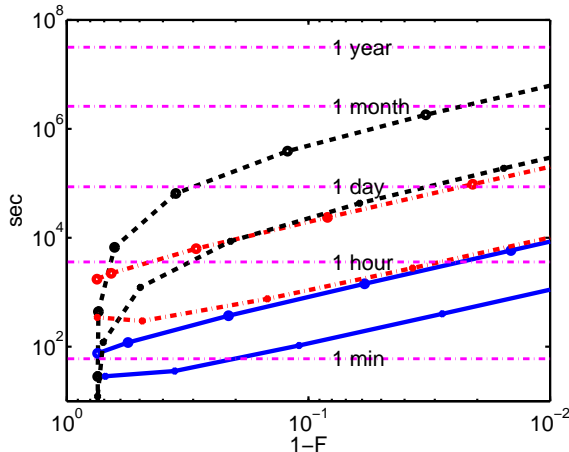


Figure 3: **Average time versus final fidelity** DLCZ (black dashed lines), new scheme without ENP (blue solid lines), and new scheme with ENP (red dashdotted lines), with efficiency  $\eta$  to be 90% (circles), and 95% (stars). Distances are 1280 km, and there is neither dynamical phase error nor misalignment.

with distance, due to the instability of the vacuum component. For our new scheme, it scales *exactly polynomially* with distance,  $t_{avg} \propto L^\alpha$ , and the exponent  $\alpha = \alpha(\eta)$  explicitly depends on the efficiency  $\eta$  (see Methods). In addition, the ENG can be much faster in our new scheme, because the requirements for initial entanglement are relaxed (Fig. 2(b)).

We examine this speed up by considering the role of errors, starting with how imperfections due to inefficiency limit the protocols. Primarily, inefficiency takes logical states into two types of nonlogical states – those with too few excitations (*vacuum* type) and those with too many excitations (*multi-excitation* type). For the DLCZ scheme the probability distribution (among the logical, vacuum and multi-excitation types) is not stable—the vacuum probability increases with distance and soon the vacuum type nonlogical state becomes the dominant term, which reduces the success probability of ENC at higher levels significantly (Fig. 2(b)). For our new approach, however, we find that the probability distribution remains stable for all higher levels of ENC (see Methods). In essence, by requiring at least one excitation in the ensemble, our qubit subspace is automatically purified of vacuum and multi-excitation type errors during ENC. The closest analog to the DLCZ scheme is our new scheme without ENP, i.e., only ENC. Our scheme is faster initially because we can start with a larger fraction of multi-excitation states but still give the same post-selection fidelity as DLCZ. At longer distances, our approach is further improved in comparison to the DLCZ scheme due to the reduced amplitude of vacuum terms.

Given fixed efficiency  $\eta$  and final fidelity  $F$ , we can optimize the excitation probability  $p_c$  to obtain the minimum  $t_{avg}$  in the presence of inefficiency errors. Such  $t-(1-F)$  curves are plotted for three different schemes and different values of  $\eta$  in Fig. 3, assuming there is

little interferometric pathlength fluctuation. Our new scheme (without ENP) is about 1000 times faster than the DLCZ scheme, for  $\eta = 90\%$ . As given by the previous discussion, this improvement is due to better control of imperfections due to inefficiency.

Besides inefficiency there are other imperfections which preserve the number of excitations but induce errors within the logical subspace, such as interferometric pathlength fluctuation and linear optical misalignment. For example, the interferometric pathlength fluctuation (with stochastic phase difference  $\delta$ ) leads to phase error (undesired logical state  $|\Psi^-\rangle$ ) with probability proportional to the variance of the phase fluctuation  $p_{phase-err} \sim \langle \delta^2 \rangle$ . This error will be amplified (doubled) during each subsequent level of ENC, because the survival probability of the state  $\Phi^-$  (the logical error) is about twice as much as that of  $\Phi^+$  (the desired component). In practice, we need interferometric phase fluctuation  $\langle \delta^2 \rangle \lesssim 1\%$  over the time to do ENG, so that  $p_{phase-err} \lesssim 1\%$ . Also, a small probability of linear optical misalignment per ENC or ENP step is modeled as depolarizing errors. Later, we will demonstrate that errors within the logical subspace restrict the final fidelity of the DLCZ scheme, while for our new approach additional active purification can correct such logical errors to achieve high fidelity.

In the presence of substantial pathlength fluctuations leading to dynamical phase errors, we plot in Fig. 4 the average time for our approach with and without ENP, the former with one phase-ENP after the second level of ENC. There is a time overhead for the new scheme with ENP as compared to the our approach without ENP. Within each scheme, the higher the efficiency  $\eta$ , the faster the quantum repeater. For high final fidelity ( $1-F \leq 10\%$ ), the curves approach straight lines with slope  $-1$ , simply because  $t \propto p_c^{-1} \propto (1-F)^{-1}$ .

Another key feature of the new scheme is its compatibility to correct errors within the logical subspace, in particular interferometric pathlength fluctuation. If such fluctuation (inducing initial phase error) is non-negligible, active ENP is indispensable. In Fig. 4,  $t-(1-F)$  curves are plotted assuming initial phase error probability  $p_{phase-err} = 1\%$ . Compared to Fig. 3, the new ingredient of initial phase error leads to an upper bound in final fidelity for all schemes. Both DLCZ and new scheme (without ENP) are limited by the initial phase error, with final fidelity no more than 65%, while new scheme (with ENP) excels in maintaining high final fidelity even up to 96%. For high retrieval and detection efficiency ( $\eta = 95\%$ ), new scheme (with ENP) can produce an entangled pair at 1280 km with a fidelity  $> 90\%$  at a bandwidth of 2 pairs/hour.

Although the present approach shows a dramatic improvement in communication rates and robustness compared to the original DLCZ scheme, the bandwidth remains relatively slow, even when very high efficiencies and very long-lived quantum memory are assumed. While such high efficiencies might ultimately be achiev-

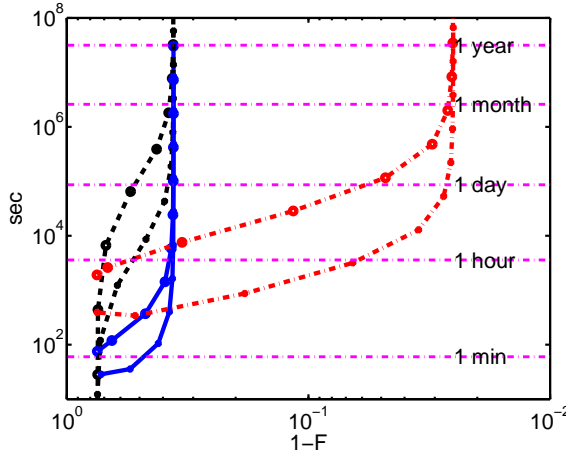


Figure 4: **Average time versus final fidelity with phase errors** This shows the same optimized approaches as Fig. 3 but with a dynamical phase error in the elementary two cell entangled state of  $p_{phase-err} \approx \frac{1}{2} \sin^2 \frac{\delta}{2} = 0.5\%$ . Inclusion of ENP (red dashdotted lines) yields a dramatic improvement in time for high fidelity operation

able (see e.g. [22] for recent progress), other approaches need to be considered that can further improve the effective communication bandwidth. For example, we can use many cells per node to improve the effective bandwidth. In this case, the improvement is at least linear with the number of cells, making it possible to realize long distance (1280 km) entangled state generation bandwidth of the order of one pair per second.[23]

The work was supported by ARO/ARDA, DARPA-QuIST, NSF Career award, NSF grant DMR-02-33773, Alfred P. Sloan Foundation, and David and Lucile Packard Foundation.

## Appendix A: METHODS

**Entanglement connection** The procedure for ENC is illustrated in Fig. 1(b). First, the spin waves stored in qubit  $b_C$  and  $a_C$  are retrieved into photons. At the lowest level of ENC, the polarization of the photons is rotated 45°. The rotations transforms  $|HV\rangle_{a_C(\text{or } b_C)}$  into  $(|HH\rangle - |VV\rangle)_{a_C(\text{or } b_C)}$ , because for bosonic fields [18]

$$S_H^\dagger S_V^\dagger \xrightarrow{45^\circ} (S_H^\dagger + S_V^\dagger)(S_H^\dagger - S_V^\dagger) = (S_H^\dagger S_H^\dagger - S_V^\dagger S_V^\dagger).$$

Thus, after the polarizing beam splitter (PBS) there will be at least two photons at one output. For incoming state  $|\Psi^{ENG}\rangle_{a_L b_C} \otimes |\Psi^{ENG}\rangle_{a_C b_R}$ , all seven terms containing two excitations in at least one pair of cells in the center repeater node (such as  $|HV\rangle_{a_C(\text{or } b_C)}$ ) do not contribute to the click patterns with one photon at each output. Five terms containing two excitations in one of the left or right repeater nodes (e.g.,  $|HV\rangle_{a_L(\text{or } b_R)}$ ) have at most

one excitation retrieved from  $b_C$  and  $a_C$ , which is insufficient to give two clicks. Therefore, only the four terms remaining can give the correct photon detector click patterns.

For all levels of ENC, the photons are then joined on the middle PBS and the number of photons at two outputs are counted in the  $\{|+\rangle, |-\rangle\}$  basis. With probability 50%, there is one photon at each output, and the connection is successful; otherwise the process is repeated. If the two photons have orthogonal polarizations, a bit flip  $\alpha|H\rangle + \beta|V\rangle \rightarrow \alpha|V\rangle + \beta|H\rangle$  is applied to  $a_L$ .[24] At higher levels of ENC, where the 45° rotations are not necessary, the bit flip is replaced by the phase flip  $\alpha|H\rangle + \beta|V\rangle \rightarrow \alpha|H\rangle - \beta|V\rangle$ .[25]

**Imperfections due to inefficiency** For our new approach, we represent two dominant types of nonlogical states by density matrix  $\pi_{vac}$  (a mixed state with at most one excitation between both pairs of cells) and  $\pi_{multi}$  (a mixed state with at least one pair of cells with more than one excitation). The normalized density matrix after  $m$ th ENC (Fig. 1(b)) can be written as

$$\rho_{a_L, b_R}^{(m)} = p_{logic}^{(m)} \rho_{logic}^{(m)} + p_{vac}^{(m)} \pi_{vac}^{(m)} + p_{multi}^{(m)} \pi_{multi}^{(m)}$$

where the  $m$ -dependent operator  $\rho_{logic}^{(m)}$  is the density matrix within logical subspace;  $\pi_{vac}^{(m)}$  and  $\pi_{multi}^{(m)}$  also depend on  $m$ ; and the coefficients  $p_{logic}^{(m)}$ ,  $p_{vac}^{(m)}$  and  $p_{multi}^{(m)}$  are the probabilities for the logical, vacuum and multi-excitation types, respectively.

After the first level of ENC,  $p_{vac}^{(1)} \sim 1 - \eta$  and  $p_{multi}^{(1)} \sim p_c \ll 1$ . We can demonstrate that these three probabilities remain stable for all higher levels of ENC, by considering the un-normalized state after  $(m+1)$ th ENC for the new approach:  $\tilde{\rho}_{a,b}^{(m+1)} = \tilde{p}_{logic}^{(m+1)} \rho_{logic}^{(m+1)} + \tilde{p}_{vac}^{(m+1)} \pi_{vac}^{(m+1)} + \tilde{p}_{multi}^{(m+1)} \pi_{multi}^{(m+1)}$ , with

$$\begin{aligned} \tilde{p}_{logic}^{(m+1)} &\approx \frac{1}{2} \eta p_{logic}^{(m)} p_{logic}^{(m)} (1 + p_{err}^{(m+1)} + O(p_{multi}^{(m+1)})) \\ \tilde{p}_{vac}^{(m+1)} &\approx \frac{1}{2} \eta p_{logic}^{(m)} p_{vac}^{(m)} (1 + O(p_{multi}^{(m+1)})) \\ \tilde{p}_{multi}^{(m+1)} &\approx \frac{1}{2} \eta p_{logic}^{(m)} p_{multi}^{(m)} (1 + O(p_{multi}^{(m+1)})) \end{aligned}$$

where the logical error probability is

$$p_{err}^{(m+1)} \sim (1 - \eta) p_{multi}^{(m)} / p_{logic}^{(m)}. \quad (A1)$$

A more detailed calculation, in which  $\pi_{vac}$  and  $\pi_{multi}$  are further divided into subspaces with different number of excitations (e.g.  $\pi_{vac}$  is subdivided into zero-excitation and one-excitation subspaces), verifies the stability of the probability distribution of  $p_{logic}^{(m)}$ ,  $p_{vac}^{(m)}$  and  $p_{multi}^{(m)}$ .[26]

For DLCZ scheme, only two cells are used to store entanglement. Besides the logical states (single excitation

in two cells), we can similarly define the vacuum states (with no excitation) and multi-excitation states (with two or more excitations). Contrary to our approach, for DLCZ the probability distribution is not stable: both vacuum and multi-excitation probabilities increases with distance. The vacuum probability soon becomes the dominant term, which reduces the success probability of ENC significantly, resulting in super-polynomial (but still sub-exponential) time scaling (Fig. 2(b)). The logical error probability for DLCZ has the same form as Eq.(A1) up to the coefficient. The quantity  $p_{multi}^{(m)}/p_{logic}^{(m)}$  (and  $p_{err}^{(m)}$ ) grows with distance, which accounts for the sharp decrease of fidelity for DLCZ in Fig. 2(a). To maintain good final fidelity,  $p_{multi}^{(1)}$  (and  $p_c$ ) should be very small; that is why it takes much longer time for DLCZ to generate an elementary pair (Fig. 2(b)).

**Interferometric phase fluctuation** We use stochastic random variable  $\delta$  to represent the phase difference due to interferometric pathlength fluctuation, which changes  $|\Psi^{ENG}\rangle_{a,b}$  into a mixture:

$$|\Psi^{ENG}\rangle_{a,b} \rightarrow e^{i\phi} (|H\rangle_a |V\rangle_b + e^{i\delta} |V\rangle_a |H\rangle_b) + |HV\rangle_a |\text{vac}\rangle_b + e^{2i\phi+i\delta} |\text{vac}\rangle_a |HV\rangle_b . \quad (\text{A2})$$

where  $\phi$  is static phase difference between left and right channels. Since the last two terms with  $|HV\rangle$  will be removed during the first level of ENC, the static phase  $\phi$  has no effect. However, the probability of being in an undesired logical state  $|\Psi^-\rangle$  is  $\sin^2 \frac{\delta}{2}$ . The first

level of ENC with the combined two inputs of  $\Psi^-$  and  $\Psi^+$  gives  $\Phi^-$ , producing a phase error with probability  $2p_{phases-err} \approx 2 \langle \sin^2 \frac{\delta}{2} \rangle$ , proportional to the variance of the interferometric phase fluctuation.

**Time Scaling** For our new scheme (without ENP), we can use the stability of the probability distribution as described above to estimate the average time:

$$t_{avg} = t_0 (L/L_0)^{\log_2(1.5) + \log_2 \left( \frac{2(2-\eta)^4}{\eta^2(3-2\eta)} \right)} \quad (\text{A3})$$

where  $t_0 = \frac{1}{p_c \eta} \frac{L_0}{c} e^{L_0/L_{att}}$  is the elementary pair generation time,  $L_0$  is half the distance between neighboring repeater stations, and  $L$  is the final distance. The exponent comes from the success probability for ENC,  $p_{ENC} \approx \frac{\eta^2(3-2\eta)}{2(2-\eta)^4}$ . The constant 1.5 is the empirical estimate of the overhead from the waiting time to obtain two independent pairs versus the single pair. In Fig. 2(b), there is an overall factor difference between simulated data and Eq.(A3), because the success probability for the first level of ENC as found in Monte Carlo simulations is smaller than estimated above. It was shown [7] that one can always reach good final fidelity if the elementary pair generation probability  $p_c$  scales as  $L_0/L$ . Therefore, after accounting for the discrepancy for first level ENC, the average distant pair generation time scales *exactly polynomially* with distance  $t_{avg} \propto L^\alpha$ , with  $\alpha = 1 + \log_2(1.5) + \log_2 \left( \frac{2(2-\eta)^4}{\eta^2(3-2\eta)} \right)$ .

---

[1] N. Gisin, *et al.*, Quantum cryptography, Rev. Mod. Phys. **74**, 145 (2002).

[2] W. T. Buttler, *et al.*, Practical Free-Space Quantum Key Distribution over 1 km, Phys. Rev. Lett. **81**, 3283 (1998).

[3] A. Poppe, *et al.*, Practical quantum key distribution with polarization entangled photons, Opt. Express **12**, 3865 (2004).

[4] C. H. Bennett, *et al.*, Purification of noisy entanglement and faithful teleportation via noisy channels, Phys. Rev. Lett. **76**, 722 (1996); C.H. Bennett, *et al.*, Mixed-state entanglement and quantum error correction, Phys. Rev. A **54**, 3824 (1996).

[5] D. Deutsch, *et al.*, Quantum Privacy Amplification and the Security of Quantum Cryptography over Noisy Channels, Phys. Rev. Lett. **77**, 2818 (1996).

[6] H.-J. Briegel, *et al.*, Quantum repeater: The role of imperfect local operations in quantum communication, Phys. Rev. Lett. **81**, 5932 (1998); W. Dür, *et al.*, Quantum repeaters based on entanglement purification, Phys. Rev. A **59**, 169 (1999).

[7] L. M. Duan, M. D. Lukin, J. I. Cirac and P. Zoller, Long-distance quantum communication with atomic ensembles and linear optics, Nature **414**, 413 (2001).

[8] J. I. Cirac, *et al.*, Quantum State Transfer and Entanglement Distribution among Distant Nodes in a Quantum Network, Phys. Rev. Lett. **78**, 3221 (1997).

[9] L. M. Duan and H. J. Kimble, Scalable Photonic Quantum Computation through Cavity-Assisted Interactions, Phys. Rev. Lett. **92**, 127902 (2004).

[10] B. B. Blinov, *et al.*, Observation of entanglement between a single trapped atom and a single photon, Nature **428**, 153 (2004).

[11] L. I. Childress, *et al.*, Fault-tolerant quantum repeaters with minimal physical resources and implementations based on single-photon emitters, Phys. Rev. A **72**, 052330 (2005); L. I. Childress, *et al.*, Fault-Tolerant Quantum Communication Based on Solid-State Photon Emitters, Phys. Rev. Lett. **96**, 070504 (2006).

[12] C. W. Chou, *et al.*, Measurement-induced entanglement for excitation stored in remote atomic ensembles, Nature **438**, 828 (2005).

[13] T. Chanelière, *et al.*, Storage and retrieval of single photons transmitted between remote quantum memories, Nature **438**, 833 (2005).

[14] M. D. Eisaman, *et al.*, Electromagnetically induced transparency with tunable single-photon pulses, Nature **438**, 837 (2005).

[15] M. D. Lukin, Colloquium: Trapping and manipulating photon states in atomic ensembles, Rev. Mod. Phys. **75**, 457 (2003).

[16] J. W. Pan, *et al.*, Experimental entanglement purification of arbitrary unknown states, Nature **423**, 417 (2003).

[17] E. Knill, R. Laflamme, and G. J. Milburn, A scheme for efficient quantum computation with linear optics, *Nature* **409**, 46(2001).

[18] E. Merzbacher, *Quantum Mechanics* (John Wiley & Sons, Inc., 1998).

[19] M. D. Eisaman, *et al.*, Shaping Quantum Pulses of Light Via Coherent Atomic Memory, *Phys. Rev. Lett.* **93**, 233602 (2004).

[20] ENP can be summarized as  $\Theta_{ENP}^{m,m'} |x\rangle_{a_1} |y\rangle_{b_1} |u\rangle_{a_2} |v\rangle_{b_2} \rightarrow (x \oplus u \oplus 1) (y \oplus v \oplus 1) (-1)^{x \cdot (mm'+1)} |x\rangle_{a_4} |y\rangle_{b_4}$  with binary basis  $\{|0\rangle, |1\rangle\}$  for  $\{|H\rangle, |V\rangle\}$  during bit-ENP and  $\{|+\rangle, |-\rangle\}$  during phase-ENP, and  $mm'$  represents the parity of two detected photons.

[21] T. Yamamoto, *et al.*, Experimental extraction of an entangled photon pair from two identically decohered pairs, *Nature* **421**, 343 (2003).

[22] James K. Thompson, Jonathan Simon, Huanqian Loh, Vladan Vuletić, A High-Brightness Source of Narrowband, Identical-Photon Pairs, *Science* **313**, 74 (2006).

[23] A simple Monte Carlo optimization of efficient use of the cells shows that we can increase the bandwidth by a factor of  $r = M^{1.12}$ , where  $M$  is the increment of factor of physical resources.

[24] The bit and phase flips called for in ENC and ENP can be performed using linear optics the next time the qubits are retrieved from the quantum memory.

[25] ENC can be summarized as  $\Theta_{ENC}^{m,m'} |xy\rangle_{bc} \rightarrow (x \oplus y \oplus 1) (mm')$  where  $mm'$  represents the parity of two detected photons and the logical states are  $|0\rangle = |H\rangle$  and  $|1\rangle = |V\rangle$ .

[26] Similarly, dark count can also induce errors in logical subspace with probability  $\sim p_{dark} (1 - \eta_s)$ , which is however negligible due to very low dark count probability  $p_{dark}$ .